The Astrophysical Journal, 762:99 (9pp), 2013 January 10 doi:10.1088/0004-637X/762/2/99

VLASOV SIMULATIONS OF MULTI-ION PLASMA TURBULENCE IN THE SOLAR WIND

D. Perrone[1], F. Valentini[1], S. Servidio[1], S. Dalena[1,2], and P. Veltri[1]
[1] Dipartimento di Fisica and CNISM, Università della Calabria, I-87030 Rende (CS), Italy
[2] Bartol Research Institute, Department of Physics and Astronomy, University of Delaware, Newark, DE 19716, USA
Received 2012 July 23; accepted 2012 November 18; published 2012 December 19

ABSTRACT

Hybrid Vlasov–Maxwell simulations are employed to investigate the role of kinetic effects in a two-dimensional turbulent multi-ion plasma, composed of protons, alpha particles, and fluid electrons. In the typical conditions of the solar-wind environment, and in situations of decaying turbulence, the numerical results show that the velocity distribution functions of both ion species depart from the typical configuration of thermal equilibrium. These non-Maxwellian features are quantified through the statistical analysis of the temperature anisotropy, for both protons and alpha particles, in the reference frame given by the local magnetic field. Anisotropy is found to be higher in regions of high magnetic stress. Both ion species manifest a preferentially perpendicular heating, although the anisotropy is more pronounced for the alpha particles, according to solar wind observations. The anisotropy of the alpha particle, moreover, is correlated to the proton anisotropy and also depends on the local differential flow between the two species. Evident distortions of the particle distribution functions are present, with the production of bumps along the direction of the local magnetic field. The physical phenomenology recovered in these numerical simulations reproduces very common measurements in the turbulent solar wind, suggesting that the multi-ion Vlasov model constitutes a valid approach to understanding the nature of complex kinetic effects in astrophysical plasmas.

Key words: methods: numerical – solar wind – turbulence

Online-only material: color figures

1. INTRODUCTION

Astrophysical plasmas are generally in a fully turbulent regime. In particular, the solar wind can be considered as a natural laboratory for studying physical processes of plasma turbulence, whose dynamic scales cannot be achieved in laboratory experiments. Collisions in the solar wind are very rare: the particle mean free path is comparable to (or larger than) the system size ($\simeq$1 AU). These properties suggest that small-scale mechanisms should be more complex than one would expect from a fluid (viscous) description.

Spacecraft measurements generally reveal that the electromagnetic field fluctuations in the solar wind are in a state of fully developed turbulence (Bruno & Carbone 2005; Marsch 2006). The power spectrum of the fluctuating fields manifests a behavior reminiscent of the $k^{-5/3}$ power law for fluid turbulence (Kolmogorov 1941; Coleman 1968; Dobrowolny et al. 1980; Tu & Marsch 1995; Goldstein et al. 1995), where here k is the wavenumber obtained by applying the Taylor hypothesis. This inertial range turbulence extends to smaller spatial scales down to a range of wavelengths where kinetic effects dominate the plasma dynamics. At these scales, different physical processes come into play, leading to spectral shape changes. The first clear spectral change appears at scales such as the ion inertial length and/or the ion Larmor radius (Leamon et al. 2000; Bourouaine et al. 2012; Bale et al. 2005), where the spectrum of the magnetic field becomes steeper (Bale et al. 2005). At the range of spatial lengths of the order of the electron kinetic scales, interpretation of the solar-wind observations is still controversial. Two different scenarios have recently been pictured: a second spectral break with an additional power-law range (Sahraoui et al. 2010) and an exponential cutoff (Alexandrova et al. 2009) that instead marks the end of self-similarity. In both cases, theoretical support from self-consistent, fully nonlinear Vlasov models is needed for the interpretation of this complex phenomenology.

This general picture of astrophysical turbulence becomes more complicated because of the multi-component nature of the solar wind. The interplanetary medium, although predominantly constituted of protons, is also made up of a finite amount of doubled ionized helium (alpha particles), together with a few percents of heavier ions. Several observations (Marsch et al. 1982a, 1982b; Kasper et al. 2008) have shown that heavier ions are heated and accelerated preferentially as compared to protons and electrons. Moreover, in a recent analysis performed on solar-wind data from the *Helios* spacecraft, the link between the signatures of kinetic effects and some important parameters of heavy ions, such as relative speed, temperature ratio, and anisotropy, has been investigated (Bourouaine et al. 2010, 2011a, 2011b). In these works, the authors pointed out that more significant anisotropies and non-Maxwellian features are detected for alpha-particle distribution functions with respect to protons. The evolution of the velocity distribution functions in the solar wind and the production of kinetic signatures such as heating and temperature anisotropies today represent some of the key issues of plasma physics (Osman et al. 2011, 2012). Recently, the problem of particle heating has also been explained in terms of non-resonant stochastic heating (Chandran et al. 2010). Moreover, this mechanism seems to have a greater efficiency for heavier ions. The above non-resonant stochastic heating predictions are further supported by fluid models in which finite Larmor radius corrections are included (Laveder et al. 2011).

The two points discussed above, that the kinetic scales have a determinant effect in shaping the turbulent spectra and that the role of secondary ions cannot be neglected, suggest that a multi-scale and multi-species self-consistent Vlasov treatment of the turbulent solar wind is required. The detec-

tion of the main kinetic processes, acting on small scales, that are responsible for the energy dissipation and heating production represents one of the main challenges for the plasma scientific community today. A kinetic description of collisionless plasma turbulence offers the powerful opportunity of giving important insights into the interpretation of "in situ" satellite measurements in the solar wind. In this context, kinetic numerical simulations are an indispensable and crucial support to investigating the complexity of solar-wind physics. The use of these simulations involves a minimal amount of physical assumptions, but of course with the drawback of limited resolution.

The most widely adopted numerical description of the kinetic plasma physics is represented by the Particle in Cell (PIC) methods. The Lagrangian PIC approach is based on the integration of the equations of motion of a large number of macro-particles under the effects of self-consistent electromagnetic fields. The PIC simulations have been extensively used for the description of the kinetic dynamics of space plasmas, addressing the problem of wave–particle interaction (Araneda et al. 2008), particle heating (Araneda et al. 2009), and turbulence (Gary et al. 2008; Saito et al. 2008; Parashar et al. 2010; Camporeale & Burgess 2011; Parashar et al. 2011; Markovskii & Vasquez 2011). Today, thanks to the fast technological development of computational resources, the Eulerian approach for the numerical solution of the Vlasov equation has become accessible as an alternative to the PIC approach (Mangeney et al. 2002). The Eulerian Vlasov simulations, in which the time evolution of the particle distribution function is followed numerically in a discretized phase space domain, are significantly more demanding computationally compared to the PIC simulations. Nevertheless, at variance with the PIC methods, the Vlasov algorithms are mostly noise-free and do not introduce additional (unphysical) heating due to the particle noise. This point can be crucial when dealing with the numerical description of the short wavelength part of the turbulent cascade, where the energy level of the fluctuations is typically very low and the statistical noise introduced by the PIC calculations can possibly cover the physical information.

Recently (Mangeney et al. 2002; Valentini et al. 2005, 2007), a Eulerian hybrid Vlasov–Maxwell code (HVM hereafter) has been developed. This algorithm numerically integrates the Vlasov equation in phase space coupled to the Maxwell equations for the electromagnetic fields. The Vlasov equation is solved for the proton species, while electrons are treated as a fluid (Valentini et al. 2007). This Eulerian approach, even though it has the major advantage of a reduced numerical noise, has restrictions regarding the numerical resolution, and therefore cannot simulate realistic inertial ranges of turbulence. The HMV code has been extensively used for the analysis of the kinetic effects during the evolution of the solar-wind cascade (Valentini et al. 2008; Valentini & Veltri 2009; Valentini et al. 2010, 2011). Furthermore, Servidio et al. (2012) made use of the HMV algorithm to investigate the role of local kinetic effects in plasma turbulence in a 2D–3V phase space configuration (two dimensions in physical space and three in velocity space). It has been shown that, near the region of strong magnetic activity, the proton distribution function is deformed by kinetic effects displaying significant non-Maxwellian features. Moreover, in these regions characterized by high magnetic stress, reconnection events can occur locally, as has also been described in both PIC and Magnetohydrodynamic simulations (Servidio et al. 2009; Drake et al. 2010).

As discussed previously, in the solar wind description, it is important to account for its multi-component nature. For this purpose, Perrone et al. (2011) have proposed an updated version of the HVM code, which includes the kinetic dynamics of heavy ions. In particular, the authors examined the effects produced by the presence of alpha particles in the evolution of the solar-wind turbulent cascade in the direction parallel to the ambient magnetic field in a 1D–3V phase space configuration.

In the present paper, we discuss the results obtained by the "multi-component" version of the HVM code in a 2D–3V phase space configuration. In order to study turbulent activity in the presence of alpha particles, we adopt an approach similar to the one used by Servidio et al. (2012), extending the above results to the more realistic multi-ion treatment. As we will discuss in the following, our numerical simulations reproduce several features commonly observed in space plasmas. As the result of the turbulent cascade, coherent structures appear in the system, with regions of high magnetic stress where reconnection occurs locally; the particle distribution functions corresponding to these regions are heavily distorted, exhibiting a significant temperature anisotropy. This effect is more evident for alpha particles than for protons, consistent with recent observations in the solar wind (Bourouaine et al. 2010, 2011b).

2. NUMERICAL MODEL

We simulate a collisionless and magnetized multi-species (electrons, protons, and alpha particles) turbulent plasma through the use of the HVM code. Within this HVM model, the Vlasov equation for proton (f_p) and alpha particle (f_α) distribution functions (Valentini et al. 2007; Perrone et al. 2011) is integrated numerically in a 2D–3V phase space domain. Electrons are treated as a fluid and a generalized Ohm equation, where a resistive term has been added as a standard numerical Laplacian dissipation, is considered. The dimensionless HVM equations are given by

$$\frac{\partial f_i}{\partial t} + \mathbf{v}\cdot\frac{\partial f_i}{\partial \mathbf{r}} + \zeta_i(\mathbf{E}+\mathbf{v}\times\mathbf{B})\cdot\frac{\partial f_i}{\partial \mathbf{v}} = 0, \tag{1}$$

$$\mathbf{E} = -(\mathbf{u}_e\times\mathbf{B}) - \frac{1}{n_e}\nabla P_e + \eta\mathbf{j}, \tag{2}$$

$$\frac{\partial \mathbf{B}}{\partial t} = -\nabla\times\mathbf{E}. \tag{3}$$

The quasi-neutrality approximation $n_e = \sum_i Z_i n_i$ is considered, where n_e and n_i are the electron and ion densities, respectively, and Z_i is the ion charge number (the subscript $i = p, \alpha$ stands for protons and alpha particles, respectively). In Equation (1), $f_i(\mathbf{r}, \mathbf{v}, t)$ is the ion distribution function, $\mathbf{E}(\mathbf{r}, t)$ and $\mathbf{B}(\mathbf{r}, t)$ are the electric and magnetic fields, and ζ_i is a constant that depends on the charge to mass ratio of each ion species. In Equation (2), the electron bulk velocity is defined as $\mathbf{u}_e = (\sum_i Z_i n_i \mathbf{u}_i - \nabla\times\mathbf{B})/n_e$, where the ion bulk velocities $\mathbf{u}_i$ are evaluated as first-order velocity moments of the ion distribution function; finally, $\mathbf{j} = \nabla\times\mathbf{B}$ represents the total current density. An isothermal equation of state for the electron pressure P_e closes the system.

In Equations (1)–(3), time is scaled by the inverse proton-cyclotron frequency $\Omega_{\rm cp}^{-1}$, velocities by the Alfvén speed V_A, lengths by the proton skin depth $d_p = V_A/\Omega_{\rm cp}$, and masses by the proton mass m_p. From now on, all physical quantities will be expressed in units of the characteristic parameters listed

above. A small value for the resistivity ($\eta = 2 \times 10^{-2}$) has been chosen in order to achieve relatively high Reynolds numbers and to remove any spurious numerical effects due to the presence of strong current sheets. The choice of this small value for the resistivity would correspond to a very small correction, confined at small scales. This dissipation electric field $\eta \mathbf{j}$ only becomes dominant at $k_\perp d_p > 9$. As can be seen in Figure 4, this does not affect the inertial range properties of turbulence. The initial equilibrium consists of a plasma composed of kinetic protons and alpha particles, with Maxwellian velocity distributions and homogeneous densities ($n_{0,p}$ and $n_{0,\alpha}$, respectively), and fluid electrons embedded in a background magnetic field $\mathbf{B}_0 = B_0 \mathbf{e}_z$. The plasma dynamics and the development of turbulence are investigated in a double periodic (x, y) domain perpendicular to $\mathbf{B}_0$, where the total magnetic field can be written as $\mathbf{B} = \mathbf{B}_0 + \mathbf{B}_\perp$.

The equilibrium configuration is perturbed by a 2D spectrum of fluctuations for the magnetic and proton velocity fields (alpha particles have zero initial bulk velocity). We inject energy with random phases and wavenumbers in the range $0.1 < k < 0.3$, where $k = 2\pi m/L$, with $2 \leqslant m \leqslant 6$ and L being the box size in each spatial direction. The rms of the initial magnetic perturbations is $\delta B/B_0 \simeq 0.3$. Neither density disturbances nor parallel variances are imposed at $t = 0$. The proton plasma beta is $\beta_p = 2{v_{\mathrm{th},p}}^2/V_A^2 = 2$ (where $v_{\mathrm{th},p} = \sqrt{T_p/m_p} = 1$ is the proton thermal speed) and the electron to proton temperature ratio is $T_e/T_p = 1$. For the alpha particles, we set $Z_\alpha = 2$, $m_\alpha/m_p = 4$, $n_{0,\alpha}/n_{0,p} = 5\%$, and $T_\alpha/T_p = 1$. With this choice, $\zeta_p = 1$ and $\zeta_\alpha = 1/2$ and the alpha-particle thermal speed is $v_{\mathrm{th},\alpha} = v_{\mathrm{th},p}/2$.

The system size in the spatial domain is $L = 2\pi \times 20 d_p$ in both x and y directions, while the limits of the velocity domain for both ion species are fixed at $v_{\mathrm{max},i} = \pm 5 v_{\mathrm{th},i}$ in each velocity direction. In these simulations, we use 512^2 grid-points in the 2D spatial domain and 61^3 and 31^3 grid-points in proton and alpha-particle three-dimensional (3D) velocity domains, respectively. We point out that in the Ohm equation for the electric field, we have neglected the electron inertia terms. These terms are in fact proportional to the squared electron skin depth (which in scaled units is given by $d_e^2 = m_e/m_p$), which cannot be adequately resolved within the discretization of our simulations. The time step Δt has been chosen in such a way that the Courant–Friedrichs–Lewy condition for the numerical stability of the Vlasov algorithm is satisfied (Peyret & Taylor 1986).

3. NUMERICAL RESULTS

We numerically study the kinetic evolution of protons and alpha particles in a situation of decaying turbulence. We expect that kinetic effects develop simultaneously with magnetic fluctuations and shears, with the latter playing a fundamental role in the production of interesting features such as particle acceleration, heating, temperature anisotropy, wave–particle like interactions, and generation of beams in the ion distribution function.

As in the fluid counterpart, large-scale fluctuations produce a turbulent cascade toward small scales (high k's). Analogously with fluid models (MHD, Hall MHD, etc.) of decaying turbulence (Mininni & Pouquet 2009), it is possible to identify an instant of time at which the turbulent activity reaches its maximum value. Since the current density is proportional to the level of small-scale gradients, a good indicator of the level of turbulent activity is represented by the average out-of-plane

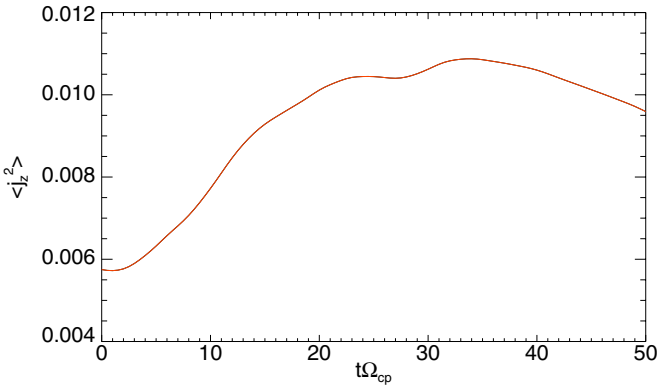

Figure 1. Time evolution of the average out-of-plane squared current density $\langle j_z^2 \rangle$.

(A color version of this figure is available in the online journal.)

squared current density $\langle j_z^2 \rangle$, whose time evolution is shown in Figure 1. Evidently, at $t = t^* \sim 40$, $\langle j_z^2 \rangle$ attains its maximum value. This is the characteristic time at which decaying turbulence shares many statistical similarities with steady state (driven) turbulence, and it is at this time that we perform our analysis.

The turbulent activity leads to the generation of coherent structures. Vortices and current sheets appear in the contour plots of Figure 2, where shaded contours of the out-of-plane total current density j_z (panel (a)) are represented. In the same figure, for the descending panels, the separate contributions $j_z^{(i)}$ of each species, namely, $j_z^{(p)} = Z_p n_p u_z^{(p)}$ (proton current), being $Z_p = 1$, $j_z^{(\alpha)} = Z_\alpha n_\alpha u_z^{(\alpha)}$ (alpha-particle current), and $j_z^{(e)} = j_z^{(p)} + j_z^{(\alpha)} - j_z$ (electron current) are also shown. The contour lines in each plot represent the magnetic potential A_z of the inplane magnetic field ($\mathbf{B}_\perp = \nabla A_z \times \mathbf{e}_z$). The different colors (black/white) of the A_z contour lines indicate different directions of rotation for the vortices. Through a careful analysis of the four plots of Figure 2, a certain correlation seems to exist between the proton and the alpha-particle current densities, revealing that the local small-scale structures of the two ion species behave in a similar way. Moreover, the electron flow generates structures at smaller scales, manifesting a more intermittent and bursty character. The coherent structures visible in the four plots of Figure 2 are not static, but evolve in time, interacting nonlinearly among each others. Moreover, in between the islands, the current becomes very intense and magnetic reconnection events locally occur at the X points of A_z, indicated in the contour plot of panel (a) by black crosses. The presence of these high magnetic stress regions is a signature of the intermittent nature of the magnetic field, which also affects the patchiness of the parallel and perpendicular heating (see below).

In the top panel of Figure 3, we report the probability distribution functions (PDFs) of $j_z^{(p)}$ (blue dashed-square line), $j_z^{(\alpha)}$ (green dashed-circle line), $j_z^{(e)}$ (red solid-cross line), and j_z (black dashed-triangle line). This plot clearly indicates that there is a certain ordering in the maximum values of the achieved current. The main contribution to the total current seems to come from the electrons and the protons that develop the most intense bursty events. In contrast, the alpha-particle current structures are smoother and concentrated on larger scales, as can be seen in Figure 2. In the same figure (bottom panel), we report the PDF of the standardized variables obtained by subtracting the average and normalizing to the respective rms value. The Gaussian

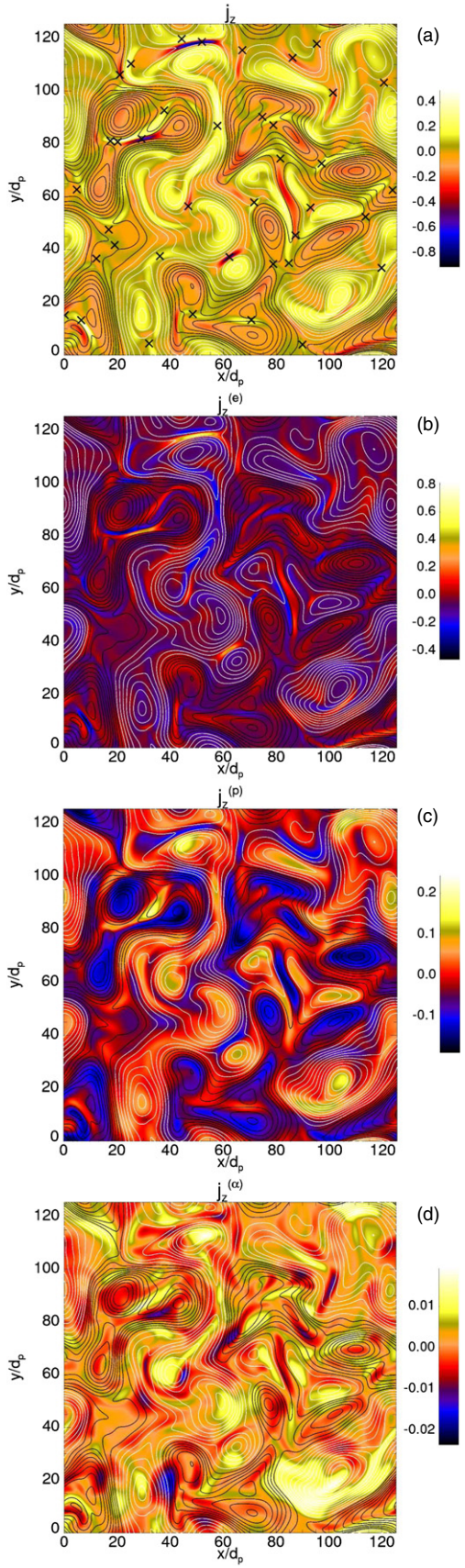

Figure 2. Contour plots (shaded colors) of the out-of-plane current densities: j_z (a), $j_z^{(e)}$ (b), $j_z^{(p)}$ (c), and $j_z^{(\alpha)}$ (d). The isolines of the magnetic potential A_z are indicated by black/white lines. In panel (a), the positions of the X-points (regions of magnetic reconnection) are indicated by black thick crosses.

(A color version of this figure is available in the online journal.)

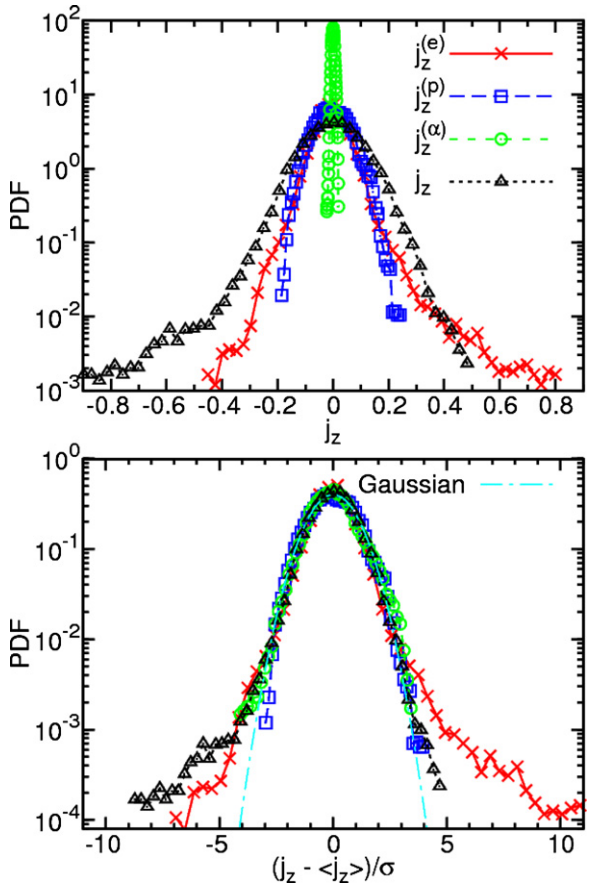

Figure 3. In the top panel, we show the PDFs of the different current densities: $j_z^{(e)}$ red solid-cross line, $j_z^{(p)}$ blue dashed-square line, $j_z^{(\alpha)}$ green dashed-circle line, and j_z black dashed-triangle line. In the bottom panel, the PDFs of the standardized variables, obtained by subtracting the average and normalizing to the respective rms value, are reported. The light-blue dot-dashed line is the Gaussian fit.

(A color version of this figure is available in the online journal.)

fit is also plotted (light-blue dot-dashed line) for reference. The currents j_z and $j_z^{(e)}$ are highly non-Gaussian distributed, because they are related to the increments (gradients) of the magnetic field (and electron flows are essentially frozen-in). The proton and alpha-particle contributions, on the other hand, behave more like Gaussian variables, since they are related to primitive variables of turbulence such as velocities and densities, and they do not capture high-order statistics.

In order to quantify the turbulence, the power spectra of the density and bulk velocity for both protons and alpha particles and of the magnetic and electric fields have been computed. In Figure 4, we show the power spectra of n_p (green-square line), $\mathbf{u}_p$ (purple-triangle line), $\mathbf{B}$ (black-solid line), and $\mathbf{E}$ (red-dashed line). The Kolmogorov expectation $k^{-5/3}$ (black-dashed line) has been plotted in Figure 4 for reference. These omnidirectional power spectra reveal several interesting features, many of which are also recovered in solar-wind spacecraft observations. First, the large scale activity is incompressible. This is also related to the fact that the system is 2D, in a plane perpendicular to the mean magnetic field (therefore inhibiting the magnetosonic activity). Second, the Alfvènic correlation between magnetic and velocity fluctuations is broken at the proton skin depth (vertical black dashed line). Moreover, the electric activity (red-dashed line) at higher wavenumbers is significantly more intense than the magnetic one (black-solid line; Bruno & Carbone 2005; Bale et al. 2005). It is worth pointing out that the

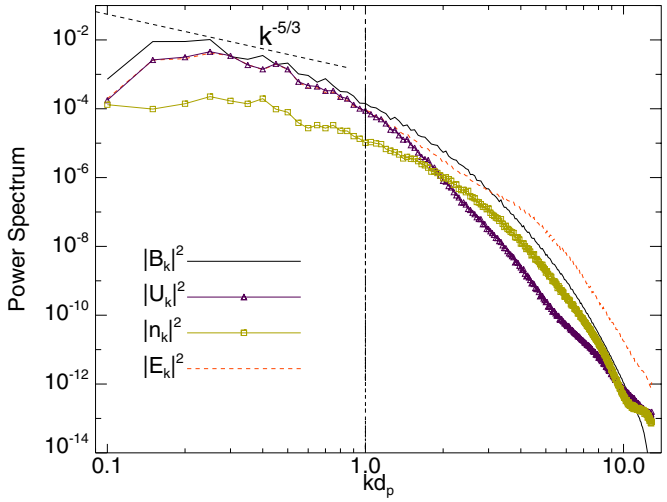

Figure 4. Power spectra of n_p (green-square line), $\mathbf{u}_p$ (purple-triangle line), **B** (black-solid line), and **E** (red-dashed line).
(A color version of this figure is available in the online journal.)

power spectra displayed in Figure 4 present no significant differences with respect to the same spectra obtained through HVM simulations without alpha particles (see Figure 1(b) in Servidio et al. 2012), meaning that the presence of alpha particles does not significantly affect the dynamical evolution of the turbulent cascade. To make a direct comparison of the dynamical evolution of the two ion species, in Figure 5, we show the velocity spectra $|U_k^{(i)}|^2$ (panel (a)) and the normalized density spectra $|N_k^{(i)}|^2$ (panel (b)) for protons ($i = p$, black-solid lines) and for alpha particles ($i = \alpha$, red-dashed lines). The density spectra for protons and alpha particles are normalized to $n_{0,p}$ and $n_{0,\alpha}$, respectively. While the velocity spectra (panel (a)) of the two ion species do not display significantly different features, we note that the alpha-particle contribution to the density spectra (panel (b)) is lower than the proton one for wavenumbers higher than the proton skin depth wavenumber. This behavior is possibly related to the fact that the alpha particles are heavier than protons, so their inertia does not allow them to follow the field fluctuations at smaller scales.

At this point, it is important to investigate the link between the turbulent behavior observed in the plasma and the generation of non-Maxwellian features in velocity space. For this purpose, the ion temperature anisotropy for each species $A_i = T_\perp^{(i)}/T_\parallel^{(i)}$, defined as the ratio between the perpendicular and the parallel temperature with respect to the local magnetic field, has been computed. Our initial condition has been set up in such a way to have spatially isotropic temperatures for both of the ion species at $t = 0$. Nevertheless, during the development of turbulence, the temperatures do not remain spatially isotropic but present local enhancements and depressions near the regions of high magnetic stress (not shown), as already found for the protons in Servidio et al. (2012).

Figure 6 shows the PDF of the temperature anisotropy for protons A_p (panel (a)) and alpha particles A_α (panel (b)) at four different times in the simulation. In the early stage of the system evolution ($t = 1$ black line), the PDFs are picked around $A_p = A_\alpha = 1$, meaning that the simulation starts with an isotropic configuration. During the evolution of the system ($t = 21$, purple line; $t = 34$, red line; $t = 40$, blue line), the PDFs elongate in the parallel ($A_i < 1$) and in the perpendicular ($A_i > 1$) direction, displaying a strong anisotropic behavior. It

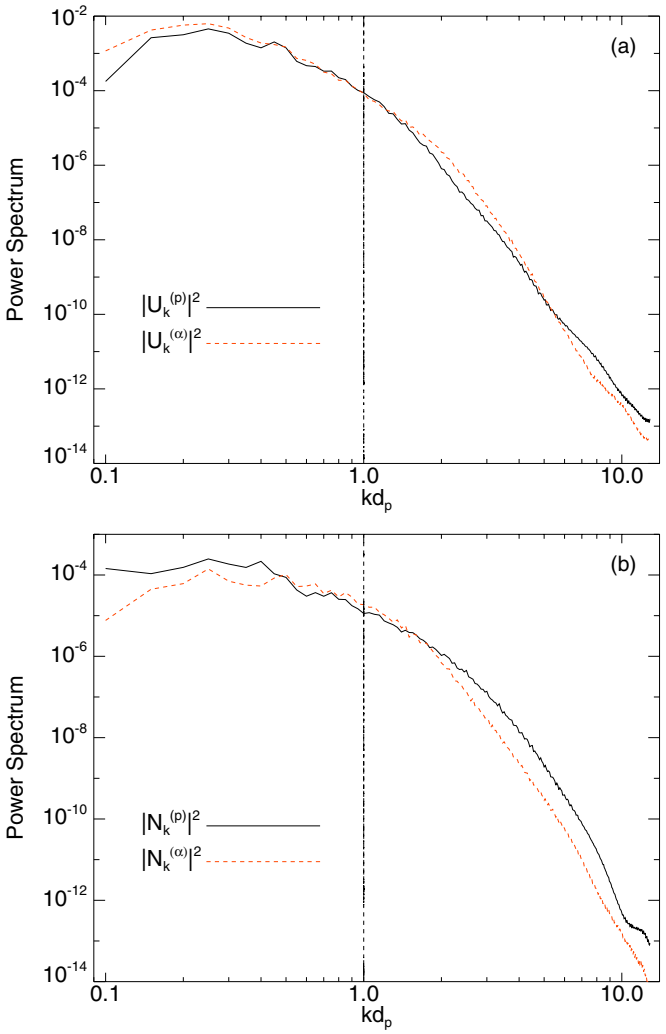

Figure 5. Panel (a): power spectra $|U_k^{(i)}|^2$ of the proton bulk velocity ($i = p$, black-solid line) and of the alpha-particle bulk velocity ($i = \alpha$, red-dashed line); panel (b): power spectra $|N_k^{(i)}|^2$ of the proton density ($i = p$, black-solid line) and of the alpha-particle density ($i = \alpha$, red-dashed line).
(A color version of this figure is available in the online journal.)

is worth noting that the statistical behavior of the anisotropies already saturates at $t \simeq 20\Omega_{\rm cp}^{-1}$. Regardless of the particular ion species, the anisotropy preferentially manifests itself along the perpendicular direction, a piece of evidence commonly detected in the solar-wind observations (Bourouaine et al. 2010, 2011b). However, alpha particles are more anisotropic than protons, as is more clearly shown in Figure 6 (bottom plot), where we have directly compared the PDFs of the two ion species (A_p black line and A_α red line) when the peak of the nonlinear activity is reached ($t = 40\Omega_{cp}^{-1}$).

A question now naturally occurs: are these patchy anisotropies correlated? Any correlation between A_α and A_p may reveal that simultaneous kinetic instabilities locally occur, modulated by the ambient magnetic field, or that an instability for a given species may influence the other, and vice versa. In Figure 7, we analyze the correlation between protons and alpha-particle temperature anisotropy, showing the joint PDF. Although most of the events are concentrated at $A_p = A_\alpha = 1$ (isotropy) and are broadly scattered because of turbulence, this joint distribution suggests that there is a clear monotonic dependency between alpha and proton anisotropies. The shape of

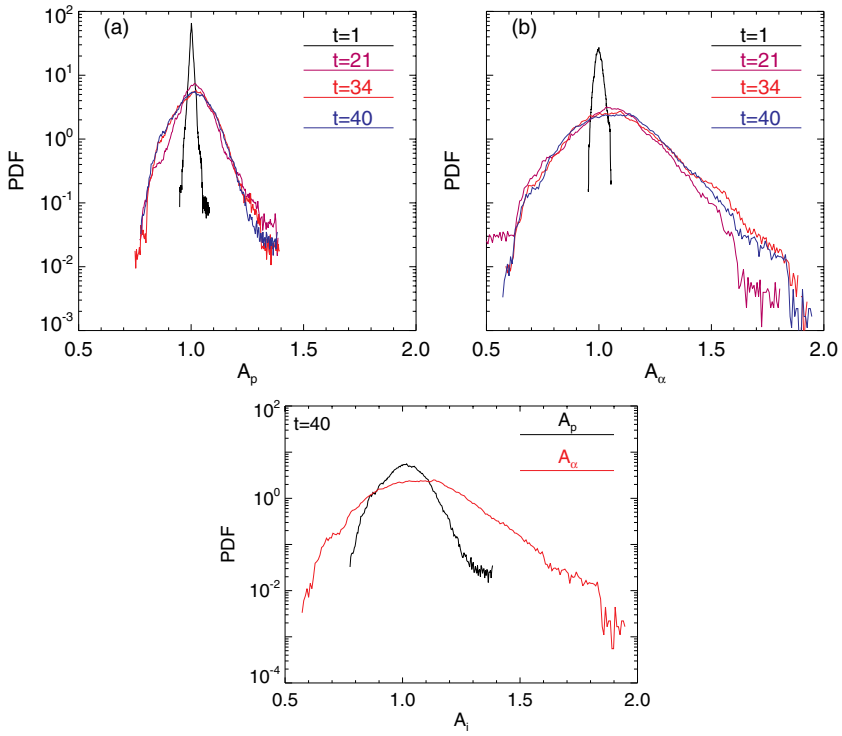

Figure 6. Top panel: PDF of the temperature anisotropy $A_i = T_\perp^{(i)}/T_\parallel^{(i)}$ of protons (a) and alpha particles (b) at four different times in the system evolution: $t = 1$ black line, $t = 21$ purple line, $t = 34$ red line, and $t = 40$ blue line. Bottom panel: comparison between the proton (A_p, black line) and the alpha-particle (A_α, red line) anisotropies is reported at the peak of the turbulent activity, i.e., at $t = 40$.

(A color version of this figure is available in the online journal.)

this distribution is in good agreement with solar wind data, as can be seen by comparing our Figure 7 with Figure 1 of Maruca et al. (2012). Moreover, analogously to Maruca et al. (2012), we fitted the above distribution with $A_p = A_\alpha^\mu$, obtaining $\mu \simeq 0.22$ (note that in Maruca et al. 2012 the authors obtained $\mu \simeq 0.25$). These results suggest that the correlation between proton and alpha-particle kinetic effects, commonly observed in the solar wind, may be the result of an active turbulent cascade, where kinetic instabilities are locally activated and modulated by the ambient magnetic field.

In a multi-ion plasma, another source of instability is represented by the differential flow between different ion species (Gary 1993; Gary et al. 2006, 2008). We found that the temperature anisotropy for the alpha particles shows a certain correlation to their drift velocity with respect to protons, $V_{\alpha p} = |\mathbf{u}_p - \mathbf{u}_\alpha|$. Analogously with fluid theory, a finite force $\mathbf{F} = Z_\alpha \mathbf{V}_{\alpha p} \times \mathbf{B}_0$ exists if the differential flow between alpha and proton velocities is not parallel to the local magnetic field. Higher differential flows, because of the induced electric field, perturb the velocity distribution functions, and vice versa. The correlation is visible in Figure 8, where we report A_α as a function of $V_{\alpha p}$: the temperature anisotropy increases with increasing relative flow speeds (in Alfvénic units) up to $V_{\alpha p} \sim 0.5$.

These results are again in good agreement with some observational analyses. Bourouaine et al. (2011b) studied correlations of temperature anisotropies and differential ion speed in the solar-wind measurements from the *Helios* spacecraft; for the case of the alpha particles, they found that A_α increases as the ion differential speed stays below about $0.5V_A$. Beyond this value, A_α becomes roughly constant, until $V_{\alpha p}$ exceeds a value of about $0.7V_A$, but then it decreases toward a value below unity when $V_{\alpha p} \simeq V_A$ (not reached in our system). Comparing our Figure 8

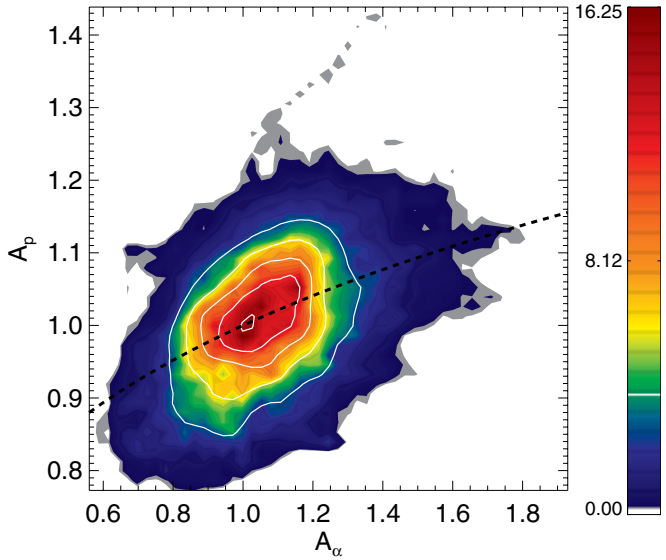

Figure 7. Joint probability distribution function of proton and alpha-particle temperature anisotropy. This two-dimensional PDF shows a correlation between the anisotropy in the two species. The best-fit $A_p \sim A_\alpha^\mu$, with $\mu = 0.22$, is also reported with a thick solid line. This behavior is in good agreement with solar wind data, as can be seen by comparing this plot with Figure 1(b) in Maruca et al. (2012).

(A color version of this figure is available in the online journal.)

with Figure 4 of Bourouaine et al. (2011b), we find a very good correspondence. However, it is worth pointing out that in a different data analysis of Advanced Composition Explorer (ACE) solar wind observations, Kasper et al. (2008) found that the alpha temperature anisotropy is monotonically decreasing with

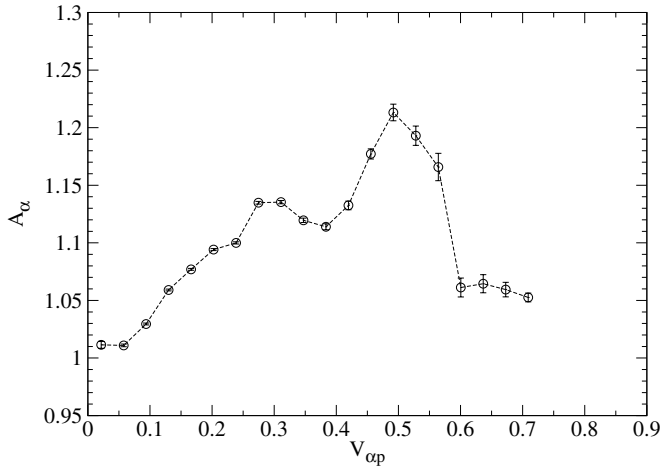

Figure 8. Anisotropy of the alpha-particle temperatures binned as a function of the differential speed $V_{\alpha p} = |\mathbf{u}_p - \mathbf{u}_\alpha|$ (in Alfvénic units). This behavior is in good agreement with solar wind observations (compare with Figure 4 of Bourouaine et al. 2011b).

increasing alpha particle to proton relative speed in the range $0 \leqslant V_{\alpha p} \lesssim 0.5$. It is also worth noting that while these studies are carried out on years of solar wind data that detect different plasmas with different parameters, homogeneities, large-scale effects and so on, in our case, these phenomena are the genuine result of a turbulent and statistically homogeneous cascade.

To conclude our study, we discuss a few examples of the effects of turbulence on the velocity distributions of alpha particles. In Figure 9, we show the iso-surfaces of the alpha-particle velocity distribution at two distinct locations in physical space, at which $A_\alpha > 1$ ((a)–(b)) and $A_\alpha < 1$ ((c)–(d)). In the same figure, we also report the direction of the local magnetic field (red tube) and the principal axis (blue tube) of the velocity distribution, evaluated from the stress tensor in the minimum variance frame (for more details see Servidio et al. 2012). The alpha-particle velocity distribution appears to be strongly affected by turbulence and modulated by the local magnetic field topology, manifesting both kinds of anisotropy; moreover, as is clear from Figure 9, the principal axis of the velocity distribution can be both aligned or perpendicular to the local magnetic field. Another interesting feature that can be appreciated in the plots of Figure 9 is the local formation of bubbles in the velocity distribution along the direction of the local magnetic field that resemble the characteristic longitudinal beams of accelerated particles commonly observed in the solar wind data (Marsch et al. 1982a, 1982b) and in 1D–3V HVM simulations (Valentini et al. 2008; Perrone et al. 2011). In these numerical papers, a possible mechanism responsible for the generation of these beams of accelerated particles has been identified in the resonant interaction of particles with a newly identified branch of electrostatic fluctuations called ion-bulk waves (Valentini et al. 2011). These resonant interaction results are more efficient for protons than for alpha particles (Perrone et al. 2011), in agreement with recent solar-wind data analysis (Marsch 2010).

4. SUMMARY AND DISCUSSION

In this paper, we discussed the numerical results of Hybrid Vlasov–Maxwell simulations employed to investigate the role

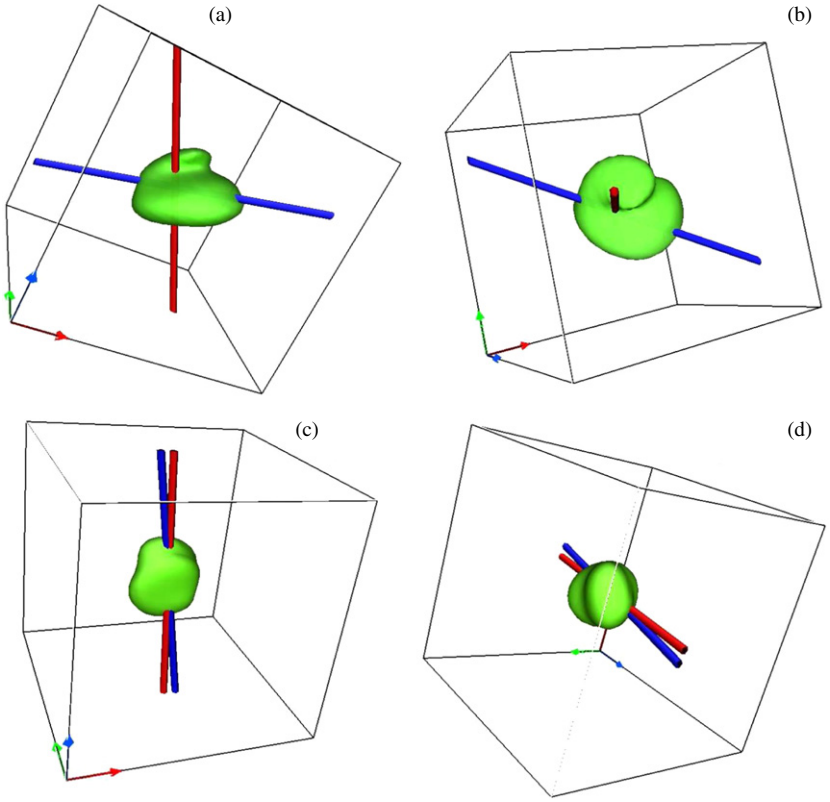

Figure 9. Iso-surfaces of the alpha-particle velocity distribution $f_\alpha(\mathbf{r}^*, v_x, v_y, v_z)$, at two different spatial locations, namely, in regions where the distribution function shows anisotropy $A_\alpha > 1$ (a)–(b) and $A_\alpha < 1$ (c)–(d). The direction of the local magnetic field (red tube) is also reported together with the principal axis (blue tube) of the velocity distribution (see Servidio et al. 2012).

(A color version of this figure is available in the online journal.)

of kinetic effects in a 2D turbulent multi-ion plasma, composed of protons, alpha particles, and fluid electrons, in the typical conditions of the solar-wind environment. While we pointed out that the presence of a small percentage of heavy ions does not affect the evolution of the turbulent cascade, our numerical results clearly show that the dynamics of alpha particles at short spatial scales display several interesting aspects, mainly consisting of the departure of the distribution function from the typical Maxwellian configuration.

In a situation of decaying turbulence, coherent structures appear, such as vortices and current sheets. In between magnetic islands, reconnection events occur. We quantify the contribution to the total current due to protons, alpha particles, and electrons, finding that most of the contribution comes from the electrons, while the current density of alpha particles is very low, due to their higher inertia. Moreover, we found that the currents of protons and alpha particles are Gaussian distributed, while electron current densities are highly intermittent, since they capture the small-scale features of the magnetic field. It is worth noting that this behavior of the electrons may also have some dependency on the equation of state used, as well as on the choice of having fluid electrons.

Power spectra for protons and for the electromagnetic fields are not too much affected by the presence of alpha particles, while at smaller scales (at k's higher than the inverse proton skin depth), the power spectrum of the alpha density has a steeper slope than that of proton density.

The non-Maxwellian features generated during the evolution of turbulence have been quantified through the statistical analysis of the temperature anisotropy in the reference frame of the local magnetic field. Note that this field, because the level of fluctuations is high, may also have a strong component in the plane, therefore allowing the presence of different types of wave-like behaviors, including whistler and Kinetic Alfvén Wave fluctuations. The joint probability distribution of the temperature anisotropies of alpha particles and protons suggests that there is a clear monotonic dependency between alpha and proton anisotropies. This reveals the occurrence of simultaneous local kinetic instabilities or the influence of the dynamical evolution of one species on the other. In general, for the parameters studied here, we found that alpha particles develop higher anisotropy than protons.

With the purpose of analyzing the role of kinetic instabilities driven by the relative speed of the two ion species, we evaluated the dependence of the temperature anisotropy of alpha particles on their drift speed $V_{\alpha p}$ with respect to protons. From this analysis, we found that the temperature anisotropy increases with increasing relative flow speeds, up to $V_{\alpha p} \simeq 0.5$ (in units of V_A). Moreover, the velocity distributions of alpha particles create bumps along the local magnetic field, resembling very common structures observed in the solar wind (Marsch 2006).

By comparing our numerical results to recent solar-wind analyses (Maruca et al. 2012; Bourouaine et al. 2011b), we found a very good quantitative correspondence both for the correlation of alpha particle and proton temperature anisotropies and for the correlation of alpha anisotropy and relative flow speed. However, it is worth noting that while the observational studies are carried out on years of solar wind data, which detect plasmas with very different features and in different physical regimes, in our case these correspondences are the genuine result of a turbulent cascade, where locally both the magnetic field topology and the relative motion of different ion flows can be the main sources of kinetic effects.

The results presented in this work significantly reproduce an important part of the complex phenomenology underlying many processes in the solar wind and suggest that a noise-free Eulerian Vlasov description of a multi-component collision-free plasma plays a fundamental role in the interpretation of the observational data from spacecraft. More work is needed on this path, including the fully 3D geometry, as well as the kinetic description of electrons.

The numerical simulations discussed in the present paper were performed within the project ASWTURB 2011 (HP10BO2REM), supported by the Italian SuperComputing Resource Allocation, ISCRA-CINECA, Bologna, Italy. S.S. acknowledges the Marie Curie Project FP7 PIRSES-2010-269297-"Turboplasmas," and the POR Calabria FSE 2007/2013. D.P. is supported by the Italian Ministry for University and Research (MIUR) PRIN 2009 funds (grant number 20092YP7EY).

REFERENCES

Alexandrova, O., Saur, J., Lacombe, C., et al. 2009, PhRvL, 103, 165003
Araneda, J. A., Maneva, Y., & Marsch, E. 2009, PhRvL, 102, 175001
Araneda, J. A., Marsch, E., & Viñas, A. F. 2008, PhRvL, 100, 125003
Bale, S. D., Kellogg, P. J., Mozer, F. S., Horbury, T. S., & Reme, H. 2005, PhRvL, 94, 215002
Bourouaine, S., Alexandrova, O., Marsch, E., & Maksimovic, M. 2012, ApJ, 749, 102
Bourouaine, S., Marsch, E., & Neubauer, F. M. 2010, GeoRL, 37, L14104
Bourouaine, S., Marsch, E., & Neubauer, F. M. 2011a, ApJL, 728, 3
Bourouaine, S., Marsch, E., & Neubauer, F. M. 2011b, A&A, 536, A39
Bruno, R., & Carbone, V. 2005, LRSP, 2, 4
Camporeale, E., & Burgess, D. 2011, ApJ, 730, 114
Chandran, B. D. G., Li, B., Rogers, B. N., Quataert, E., & Germaschewski, K. 2010, ApJ, 720, 503
Coleman, P. J. 1968, ApJ, 153, 371
Drake, J. F., Opher, M., Swisdak, M., & Chamoun, J. N. 2010, ApJ, 709, 963
Dobrowolny, M., Mangeney, A., & Veltri, P. 1980, PhRvL, 45, 144
Gary, S. P. 1993, Theory of Space Plasma Microinstabilities (Cambridge: Cambridge Univ. Press)
Gary, S. P., Saito, S., & Li, H. 2008, GeoRL, 35, L02104
Gary, S. P., Yin, L., & Winske, D. 2006, JGR, 111, A06105
Goldstein, M. L., Roberts, D. A., & Matthaeus, W. H. 1995, ARA&A, 33, 283
Kasper, J. C., Lazarus, A. J., & Gary, S. P. 2008, PhRvL, 101, 261103
Kolmogorov, A. N. 1941, DokAN, 30, 299
Laveder, D. L., Marradi, L., Passot, T., & Sulem, P. L. 2011, GeoRL, 38, L17108
Leamon, R. J., Matthaeus, W. H., Smith, C. W., et al. 2000, ApJ, 537, 1054
Mangeney, A., Califano, F., Cavazzoni, C., & Trávníček, P. 2002, JCoPh, 179, 495
Markovskii, S. A., & Vasquez, B. J. 2011, ApJ, 739, 22
Marsch, E. 2006, LRSP, 3, 1
Marsch, E. 2010, SSRv, 172, 23
Marsch, E., Mühlhäuser, K.-H., Rosenbauer, H., Schwenn, R., & Neubauer, F. M. 1982a, JGR, 87, 35
Marsch, E., Mühlhäuser, K.-H., Schwenn, R., et al. 1982b, JGR, 87, 52
Maruca, B. A., Kasper, J. C., & Gary, S. P. 2012, ApJ, 748, 137
Mininni, P. D., & Pouquet, A. 2009, PhRvE, 80, 025401
Osman, K. T., Matthaeus, W. H., Greco, A., & Servidio, S. 2011, ApJL, 727, 11
Osman, K. T., Matthaeus, W. H., Hnat, B., & Chapman, S. C. 2012, PhRvL, 108, 261103
Parashar, T. N., Servidio, S., Breech, B., Shay, M. A., & Matthaeus, W. H. 2010, PhPl, 17, 102304
Parashar, T. N., Servidio, S., Shay, M. A., Breech, B., & Matthaeus, W. H. 2011, PhPl, 18, 092302
Perrone, D., Valentini, F., & Veltri, P. 2011, ApJ, 741, 43
Peyret, R., & Taylor, T. D. 1986, Computational Methods for Fluid Flow (New York: Springer)
Sahraoui, F., Goldstein, M. L., Belmont, G., Canu, P., & Rezeau, L. 2010, PhRvL, 105, 131101
Saito, S., Gary, S. P., Li, H., & Narita, Y. 2008, PhPl, 15, 102305

Servidio, S., Matthaeus, W. H., Shay, M. A., Cassak, P. A., & Dmitruk, P. 2009, PhRvL, 102, 115003
Servidio, S., Valentini, F., Califano, F., & Veltri, P. 2012, PhRvL, 108, 045001
Tu, C.-Y., & Marsch, E. 1995, SSRv, 73, 1
Valentini, F., Califano, F., & Veltri, P. 2010, PhRvL, 104, 205002
Valentini, F., Perrone, D., & Veltri, P. 2011, ApJ, 739, 54
Valentini, F., Trávníček, P., Califano, F., Hellinger, P., & Mangeney, A. 2007, JCoPh, 225, 753
Valentini, F., & Veltri, P. 2009, PhRvL, 102, 225001
Valentini, F., Veltri, P., Califano, F., & Mangeney, A. 2008, PhRvL, 101, 025006
Valentini, F., Veltri, P., & Mangeney, A. 2005, JCoPh, 210, 730